Super band-gap time-resolved luminescence study of degenerate electron–hole plasma in thin GaAs epilayers

E. Poles, S. Y. Goldberg, B. Fainberg, and D. Huppert
Raymond and Beverly Sackler Faculty of Exact Sciences, School of Chemistry, Tel Aviv University, Ramat Aviv 69978, Israel

M. C. Hanna
National Renewable Laboratory, Golden, Colorado 80401

Y. Rosenwaks[a)]
Department of Physical Electronics, Faculty of Engineering, Tel Aviv University, Ramat Aviv 69978, Israel

(Received 30 May 1996; accepted for publication 11 July 1996)

Super band-gap time-resolved photoluminescence is employed to measure the transport properties of degenerate electron–hole gas in thin GaAs epilayers. It is found that the luminescence decay at wavelengths shorter then the energy gap wavelength is much faster then expected from a simple diffusion–reabsorption model. The results are explained by using a transport model based on Fermi–Dirac carrier statistics and nonparabolic band structure. We have found that only by introducing the above two phenomena the photoluminescence spectra at all energies can be fitted. The importance of the results in studies of hot carrier energy loss rates is discussed. © *1996 American Institute of Physics.* [S0021-8979(96)02620-5]

I. INTRODUCTION

During the last decade there has been considerable interest in photogenerated carrier dynamics in III–V semiconductors. Various issues such as hot carrier cooling,[1] minority-carrier lifetime,[2] surface recombination velocity,[3] and carrier injection across semiconductor–liquid interfaces[4] are of interest. Time-resolved photoluminescence (TRPL) is an excellent method for characterizing the above processes. In a typical experiment a short laser pulse (usually 1 ps in duration) excites the semiconductor sample with a photon energy greater than the energy band gap, creating hot carrier distributions; the electrons and holes then start to lose energy and finally reach the lattice temperature.

In general, two stages of carrier relaxation can be defined.[5,6] The initial carrier distribution at time zero after the monochromatic laser pulse is highly nonthermal due to energy and momentum selection rules for optical absorption. The first stage of carrier relaxation involves the evolution of the nonthermal distribution to a thermalized distribution, whereby the photogenerated carriers reach an equilibrium with themselves, but not with the lattice. The resulting thermalized hot carrier plasma can be assigned an effective temperature characterizing its distribution (Fermi–Dirac or Maxwell–Boltzmann). This carrier temperature is generally much higher than the lattice temperature; furthermore, the electrons and holes may equilibrate separately, leading to different temperatures for electrons and holes distributions. The second stage of carrier relaxation involves energy loss and the cooling of the thermalized hot carrier plasma to the lattice temperature. For plasma temperatures greater than 40 K, longitudinal optical (LO) photon emission is the dominant energy-loss mechanism. The characteristic time scale for this second stage of carrier cooling in bulk material is between 1 and 10 ps depending on the carrier density.[6]

One of the most widely used methods to quantify the energy loss rate of hot carriers is by measuring TRPL spectra at different PL energies above the semiconductor band gap. The spectra in the time domain are then converted to the energy domain, resulting in a family of PL versus energy spectra at various times following the excitation. The carrier temperature is then calculated by fitting each spectrum to a Fermi–Dirac carrier distribution; this gives the carrier temperature as a function of time from which the energy loss rate can be calculated.

However, due to the high optical absorption in direct gap semiconductors, carrier transport perpendicular to the layer is very fast and strongly affects the TRPL decay curves even in the sub-10 ps time regime. The transport will increase the PL decay rate at the different energies, thus leading to a change in the shape of PL versus energy spectra which are produced from the TRPL curves. The important point is that the transport may lead to a faster PL decay at a certain energy and this may be wrongly interpreted as a faster carrier cooling rate if the diffusion is neglected. This effect was recently reported by Bailey and Stanton,[7] who showed that the carrier diffusion in a thin GaAs epilayer is fast enough to affect the carrier energy distribution and hence the effective cooling rates in the first 20 ps following the laser excitation pulse. Thus, in order to obtain correct cooling rates these effects must be taken into account in the analysis of the super band-gap TRPL spectra.

In this work we address these phenomena both theoretically and experimentally in the picosecond and the nanosecond time scales. TRPL spectra were measured at several energies both on a very thin (0.5 μm) GaAs sample (where diffusion is relatively unimportant) and on a 5-μm-thick sample. We develop a rigorous model which calculates the PL decay at the super band-gap energies, taking into account

[a)]Electronic mail: yossir@post.tauc.ac.il

 0021-8979/96/80(9)/5129/9/$10.00 © 1996 American Institute of Physics

Downloaded¬30¬Mar¬2005¬to¬132.66.16.12.¬Redistribution¬subject¬to¬AIP¬license¬or¬copyright,¬see¬http://jap.aip.org/jap/copyright.jsp

the effects of carrier degeneracy and conduction-band nonparabolicity. We find very pronounced differences between the different energy luminescence spectra which can be explained only by taking into account the degeneracy and nonparabolicity effects. This implies that, in order to measure carrier cooling rates in semiconductors, such an analysis must be employed in order to avoid ''artificially'' slow energy loss rates.

The experimental techniques we have used are described in the following section. Section III describes the experimental results. The theoretical analysis is presented in Sec. IV and is compared to the luminescence spectra in Sec. V. The article is summarized in Sec. VI.

II. EXPERIMENT

The GaAs/AlGaAs heterostructures were grown by atmospheric pressure, metal-organic chemical-vapor deposition (MOCVD) at 725 °C on (100) GaAs substrates as described in detail elsewhere.[8] The samples were double-heterojunction (DH) structures that contained capping layers of nondoped $Al_xGa_{1-x}As$ ($x=0.48$) on either side of the undoped GaAs epilayer; all samples contained a 0.4 μm buffer layer of undoped GaAs. For the results reported here, two samples with different thickness of the active GaAs layers of 0.5 μm (sample A) and 5 μm (sample B) were used. The outer and inner $Al_xGa_{1-x}As$ barrier layers were 0.15 μm thick.

TRPL was measured using the time-correlated single-photon counting (TCSPC) technique. As an excitation source we used a cw mode-locked Nd:YAG-pumped dye laser (Coherent Nd:YAG Antares and a 702 dye laser) providing a high repetition rate (<1 MHz) of short pulses (2 ps). The TCSPC detection system is based on a Hamamatsu R3809U photomultiplier and the overall instrument response at full width at half-maximum was about 40 ps. The laser repetition rate and spot size were adjusted to create an initial electron–hole density not higher than 5×10^{18} cm^{-3} per pulse, in order to prevent crystal heating and surface damage. The initial excess carrier density was calculated based on the measured laser photon flux and an absorption coefficient α of 5×10^4 cm^{-1} the laser wavelength of 595 nm. The different TRPL spectra were recorded at 10 nm intervals.

III. RESULTS

A. Thin crystal photoluminescence

Figure 1 shows the TRPL curves measured at several photon energies in the range 1.43–1.75 eV (870–750 nm) of the 0.5-μm-thick GaAs sample. The absorption depth of the laser wavelength is ~2000 Å; hence, the carrier cooling and transport in the case of the thin crystal is completed within a time similar to the system instrumental response function (IRF) of 40 ps. The luminescence decay curves at energies above 1.52 eV can be divided into two main time regimes. The first is characterized by a very fast decay limited by the IRF and is attributed to the photogenerated hot carrier relaxation to the lattice temperature. The greater the photon energy, the greater is the amplitude of the shorter decay component. The cooling lasts a few picoseconds, as is usually the case with bulk III–V semiconductors. The second part of the decay curves is controlled by the radiative and nonradiative bulk recombination processes.

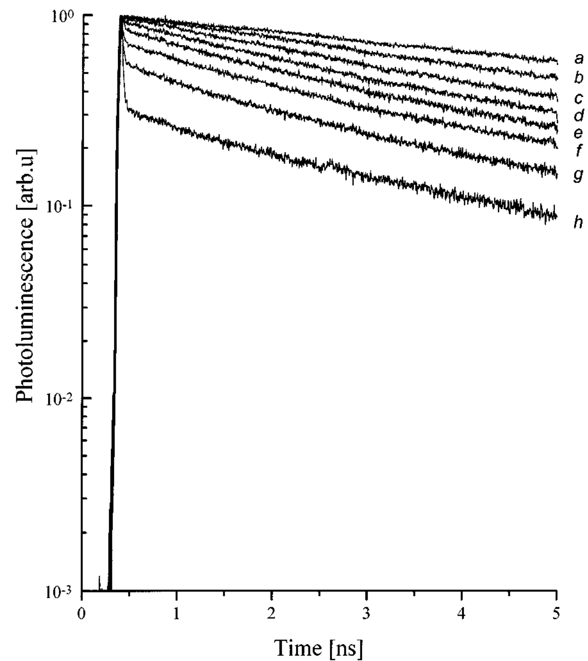

FIG. 1. Semilogarithmic plots of time-resolved photoluminescence (PL) of the thin (0.5 μm) GaAs crystal measured at various super band-gap energies of: (a) 1.45 eV; (b) 1.47 eV; (c) 1.49 eV; (d) 1.51 eV; (e) 1.53 eV; (f) 1.55 eV; (g) 1.57 eV; (h) 1.6 eV.

B. Thick crystal photoluminescence

Figure 2 shows the TRPL curves measured at selected wavelengths in the spectral range of 870–730 nm (1.43–1.65 eV) of the thick (5 μm) GaAs sample. In contrast to the TRPL curves of sample A shown above, the PL curves of the thick sample shown in Fig. 2 exhibit a multiexponential decay with three components. The breaks seen in curves (f) and (g) are due to the IRF effects; these features are more pronounced at the high photon energies due to the very fast luminescence decay. The first time period of up to 10 ps primarily reflects the cooling of the initial hot carrier distribution, and the initial diffusion process. The second time period, between several picoseconds to few nanoseconds in duration, is dominated by the transport of carriers from the initial Beer–Lambert distribution into the bulk. The third time domain, between several nanoseconds to 1 μs, is controlled primarily by the radiative and nonradiative bulk recombination processes. As can be seen from Fig. 2 the effective decay time of the transport component, (the second part of the TRPL curve) strongly depends on the PL photon energy. The larger the photon energy, (shorter PL wavelength) the smaller the effective lifetime of the transport component.

Downloaded¬30¬Mar¬2005¬to¬132.66.16.12.¬Redistribution¬subject¬to¬AIP¬license¬or¬copyright,¬see¬http://jap.aip.org/jap/copyright.jsp

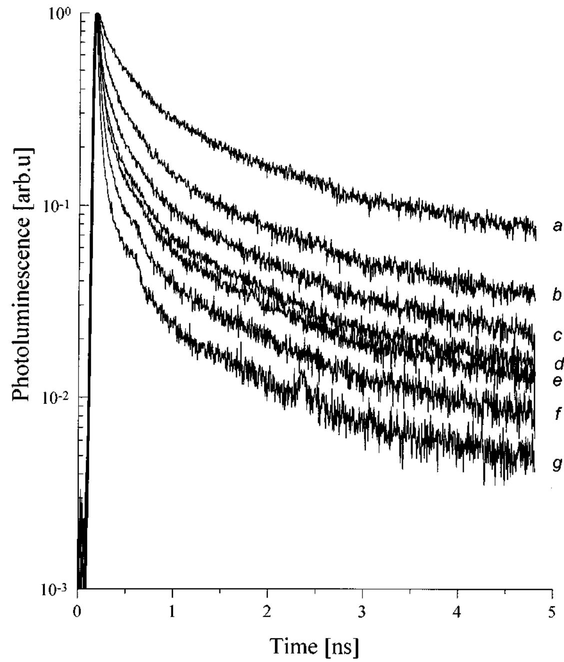

FIG. 2. Semilogarithmic plots of time-resolved photoluminescence (PL) of the thick (5 μm) GaAs crystal measured at various super band-gap energies of: (a) 1.45 eV; (b) 1.49 eV; (c) 1.53 eV; (d) 1.57 eV; (e) 1.61 eV; (f) 1.65 eV.

IV. ANALYSIS

A. Carrier transport calculated in the nondegenerate regime

The analysis in the nondegenerate regime, described in detail elsewhere,[3] is based on a numerical solution of the ambipolar diffusion equation

$$\frac{\partial \Delta n(x,t)}{\partial t} = D \frac{\partial^2 \Delta n(x,t)}{\partial x^2} + g(x,t) - \frac{\Delta n(x,t)}{\tau_B}, \tag{1}$$

with the boundary conditions

$$\left.\frac{\partial \Delta n(x,t)}{\partial x}\right|_{x=0} = \frac{S_0}{D} \Delta n(x=0,t),$$
$$\left.\frac{\partial \Delta n(x,t)}{\partial x}\right|_{x=d} = -\frac{S_0}{D} \Delta n(x=d,t), \tag{2}$$

$$\Delta n(x,t=0) = 0, \tag{3}$$

where Δn ($\Delta n = \Delta p$) is the photogenerated carrier densities at a distance x from the crystal surface and time t after excitation. D is the ambipolar diffusion constant, $g(x,t)$ the laser generation function, τ_B the effective bulk lifetime, d the epilayer thickness, and S_0 the ambipolar or intrinsic surface recombination velocity which is assumed equal at both interfaces. The use of Eq. (1) is valid only under high excitation conditions, as we have shown in the past;[9] under such conditions D and τ_B can be considered to be independent of the excess carrier concentration and the bands near the surface can be assumed to be flat. The normalized time-dependent PL intensity $I(t)$ is then calculated as

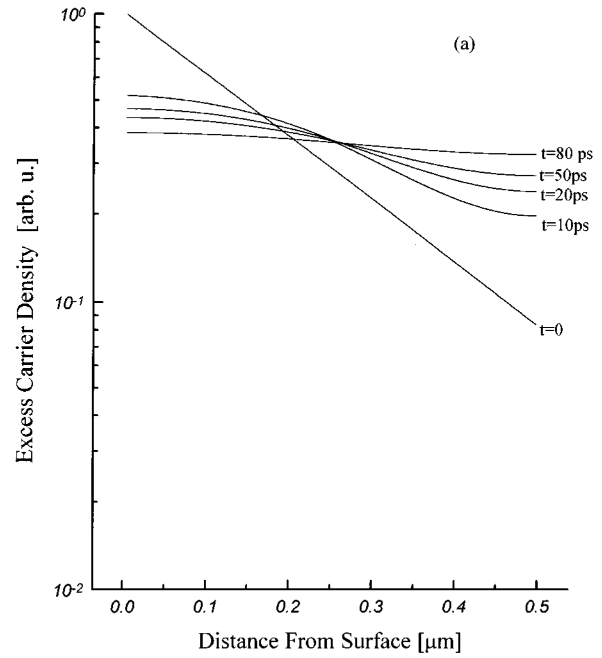

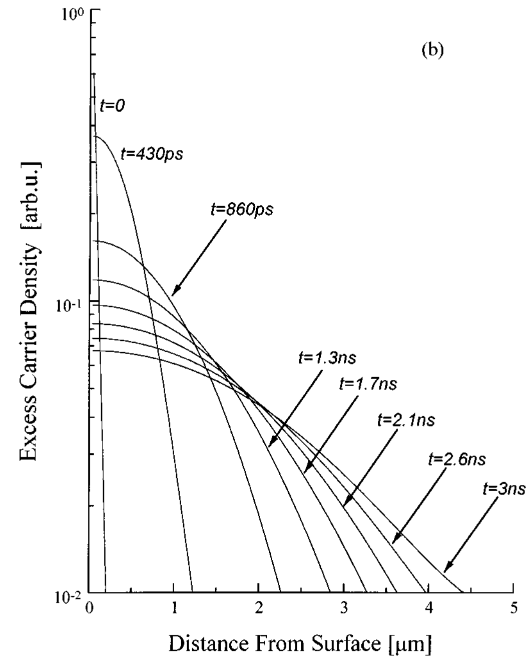

FIG. 3. (a) Computer simulations of the excess carriers spatial distribution in the thin (0.5 μm) crystal at different times: $t=0$, 10, 20, 50, and 80 ps, following the laser excitation. (b) Computer simulation of the excess carriers spatial distribution in the thick crystal, at times of: $t=0$, 430, 860, 1.3, 1.7, 2.1, 2.6, and 3 ps, following the excitation.

$$I(t) = \int_0^d \Delta n^2(x,t) \exp(-\alpha' x) dx, \tag{4}$$

where α' is the absorption coefficient at the luminescence wavelength.

The hot electron cooling process is approximated by

$$T_e = T_L + \Delta T \exp(-t/\tau_c), \tag{5}$$

where T_e and T_L are the electron and lattice temperatures, respectively. ΔT is the initial ($t=0$) temperature difference

Downloaded¬30¬Mar¬2005¬to¬132.66.16.12.¬Redistribution¬subject¬to¬AIP¬license¬or¬copyright,¬see¬http://jap.aip.org/jap/copyright.jsp

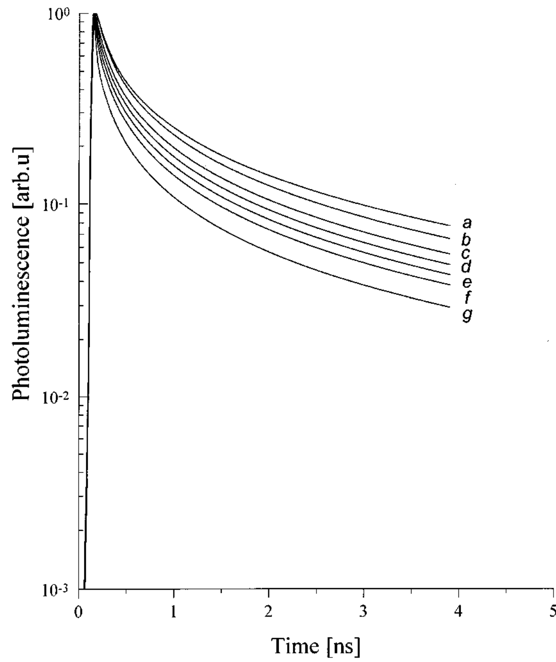

FIG. 4. Computer simulations of the photoluminescence decay using nondegenerate carrier statistics. Note the large differences between the calculations and the experimental results shown in Fig. 2. The calculated curves are at the following photoluminescence energies: (a) 1.45 eV; (b) 1.47 eV; (c) 1.49 eV; (d) 1.51 eV; (e) 1.53 eV; (f) 1.55 eV; (g) 1.57 eV.

between the electron distribution and the lattice and τ_c is a time constant characterizing the electron cooling time. τ_c is less then 10 ps for GaAs,[1] and thus is relatively short compared to our experimental time resolution. ΔT was estimated from fitting the experimental data of the thin crystal (0.5 μm); the fast cooling process is observed in the TRPL data of the thin crystal shown in Fig. 1, as a spike limited practically by our instrumental time response.

Figures 3(a) and 3(b) show calculations of the excess carrier concentration across the thin and thick samples, respectively. In the case of the thin sample the carrier distribution across the sample is nearly constant at a time of 80 ps following the excitation which means that the diffusion has a negligible effect on the PL of the thin crystal. On the other hand, it is seen that the carrier concentration across the thick sample [Fig. 3(b)] is not constant even after 3 ns, and thus diffusion will have a significant effect on the PL spectra well into the nanosecond time regime.

Figure 4 shows TRPL spectra of the thick sample calculated for different emission wavelengths using Eq. (4). The carrier cooling and the radiative and nonradiative bulk recombination processes were assumed to be identical to the ones obtained from the analysis of the thin crystal PL data. However, the experimental results (Fig. 2) show a much stronger dependence of the PL decay time on the PL wavelength then that predicted by the calculations shown in Fig. 4; it is clear that this wavelength dependence cannot be explained by the nondegenerate ambipolar diffusion model and the PL reabsorption alone and thus must be due to additional effects. These are presented in the following subsection where we develop a rigorous model which calculates the super band-gap TRPL of a semiconductor in the degenerate regime; we find an excellent agreement between the model and our experimental results.

B. Carrier transport in the degenerate regime

PL resulting from a direct radiative electron–hole recombination is commonly expressed by[10]

$$I(\hbar\omega)\sim\omega^2(\hbar\omega-E_g)^{1/2}f_ef_h, \tag{6}$$

where E_g is the energy band gap, and f_e and f_h are the electron and hole distribution functions, respectively. For times relevant to our purposes ($t>10$ ps), the distribution functions f_e and f_h can be approximated by thermalized distributions which is equivalent to assigning quasi-Fermi levels to each type of carrier.

The electron and hole energies E_e and E_h measured relative to their respective band edges are related to the photon energy $\hbar\omega$ through[5] $\hbar\omega=E_e+E_h+E_g$. Using this relation and the Fermi–Dirac distribution function Eq. (6) becomes

$$\begin{aligned}I(\hbar\omega)\sim{}&\omega^2(\hbar\omega-E_g)^{1/2}\\&\times\left\{\exp\left[\beta_e\left(\frac{m_h}{m_e+m_h}(\hbar\omega-E_g)-F_e\right)\right]+1\right\}^{-1}\\&\times\left\{\exp\left[\beta_h\left(\frac{m_e}{m_e+m_h}(\hbar\omega-E_g)-F_h\right)\right]+1\right\}^{-1},\end{aligned} \tag{7}$$

where $\beta_e=1/(kT_e)$, $\beta_h=1(kT_h)$, and m_e and m_h are the effective masses of electrons and holes, respectively; F_e and F_h are the corresponding quasi-Fermi levels, which are related to the local carrier densities n_e, n_h by

$$n_{e,h}=\frac{1}{(2\pi^3)^{1/2}}\frac{(m_{e,h}kT_{e,h})^{3/2}}{\hbar}\mathscr{F}_{1/2}(\beta_{e,h}F_{e,h}), \tag{8}$$

where

$$\mathscr{F}_n(z)=\frac{1}{\Gamma(n+1)}\int_0^\infty\frac{x^n\,dx}{\exp(x-z)+1}$$

is the nth-order Fermi integral, and the quasi-Fermi levels are measured relative to their respective band edges.

The emission spectrum is obtained by integrating $I(\hbar\omega,x,t)$ taking into account reabsorption of the luminescence,

$$I(\hbar\omega,t)=\int_0^d I(\hbar\omega,x,t)\exp[-\alpha'(\omega)x]dx, \tag{9}$$

where $\alpha'(w)$ is the absorption coefficient at a specific emission energy.

Strictly speaking, Eq. (7) is correct in the absence of transport effects. However, we shall assume the existence of local quasiequilibrium distribution functions with quasi-Fermi levels (and effective carrier temperatures) and that these distribution functions do not vary significantly over distances corresponding to the appropriate carrier mean free paths. The local carrier densities n ($n=n_e=n_h$) satisfy the ambipolar diffusion equation[11]

Downloaded¬30¬Mar¬2005¬to¬132.66.16.12.¬Redistribution¬subject¬to¬AIP¬license¬or¬copyright,¬see¬http://jap.aip.org/jap/copyright.jsp

$$\frac{\partial n}{\partial t}=\nabla(D\nabla n)+\mathscr{G}-\mathscr{R}, \tag{10}$$

where $\mathscr{G}$ and $\mathscr{R}$ are the pair generation and recombination rates, respectively. The diffusion coefficient D is given by

$$D=\mathscr{D}\left(1+n\beta[\mathscr{H}^{1/2}_{-1/2}(\beta_e F_e)+\mathscr{H}^{1/2}_{-1/2}(\beta_h F_h)]^{-1}\frac{\partial E_g}{\partial n}\right), \tag{11}$$

where

$$\mathscr{D}=\mathscr{D}^0_e\mathscr{D}^0_h\frac{T_e\mathscr{H}^{1/2}_{-1/2}(\beta_e F_e)+T_h\mathscr{H}^{1/2}_{-1/2}(\beta_h F_h)}{T_e\mathscr{D}^0_h\mathscr{H}^{1/2}_0(\beta_e F_e)+T_h\mathscr{D}^0_e\mathscr{H}^{1/2}_0(\beta_h F_h)} \tag{12}$$

is the ambipolar diffusion coefficient, $\mathscr{D}^0_e\sim T_e^{1/2}$ and $\mathscr{D}^0_h\sim T_h^{1/2}$ are the low-density electron and hole diffusion constants, respectively, and $\mathscr{H}^m_k(\beta_c F_c)=\mathscr{F}_m(\beta_c F_c)/\mathscr{F}_k(\beta_c F_c)$. The second addend in the large parentheses on the right-hand side of Eq. (11) describes the self-energy correction to the particle current,[12] which was shown to be relatively negligible at temperatures above 100 K.[12]

If the electron and the hole temperatures (T_e and T_h) are equal and coincide with the lattice temperature T, Eqs. (6)–(11) compose the whole system of equations (with corresponding boundary conditions), which permits the calculation of $I(\hbar\omega,t)$. In the case when T_e and T_h change with time (an effect which is significant only at the first 10 ps following the excitation), the hot phonon formation that increases the electron–phonon relaxation time must also be considered.[13,14]

Equations (6), (7), (10), and (11) simplify in the case of nondegenerate electron–hole gases to

$$\begin{gathered}I(\hbar\omega,x,t)\sim\omega^2(\hbar\omega-Eg)^{1/2}n_e n_h\exp[-\beta(\hbar\omega-Eg)],\\ \mathscr{H}^{1/2}_{-1/2}(\beta F_c)=\mathscr{H}^{1/2}_0(\beta F_c)=1,\end{gathered} \tag{13}$$

and

$$\mathscr{D}\approx\frac{2\mathscr{D}^0_e\mathscr{D}^0_h}{\mathscr{D}^0_h+\mathscr{D}^0_e}, \tag{14}$$

where we disregarded the self-energy correction to the particle current due to small density $n=n_e=n_h$ in the nondegenerate case.

However, Eqs. (13) and (14) fail to explain our experimental data. The main reason is that for an electron density of $n\sim3\times10^{18}$ cm^{-3} (which corresponds to our experimental conditions) and $T=300$ K the strong degeneracy condition[15] is satisfied for the electron system,

$$\beta_e F_e=\frac{\beta_e(3\pi^2 n_e)^{2/3}}{2m_e}\approx4>1, \tag{15}$$

where we have used $m_e^*=0.068m_{oe}$ for GaAs. For the heavy-hole system, the corresponding parameter $\beta_h F_h>1$, since the ratio $m_h^*/m_e^*=7.53$. The electron and hole concentrations in our experiments are around 3×10^{18} cm^{-3}; therefore, as a first-order approximation, we can consider the carrier system as degenerate for electrons, and as nondegenerate for the holes. In such a case Eq. (7) becomes

$$\begin{aligned}I(\hbar\omega,x,t)\sim{}&\omega^2(\hbar\omega-Eg)^{1/2}n_h\\ &\times\left[\exp\left(-\frac{m_e}{m_e+m_h}\beta_h(\hbar\omega-Eg)\right)\right]\\ &\times\left\{\exp\left[\left(\frac{m_h}{m_e+m_h}(\hbar\omega-Eg)-F_e\right)\right]+1\right\}^{-1},\end{aligned} \tag{16}$$

where $F_e=\hbar^2(3\pi^2 n_e)^{2/3}/(2m_e)$,

$$\begin{gathered}\mathscr{H}^{1/2}_0(\beta_e F_e)=\frac{4}{3\sqrt{\pi}}(\beta_e F_e)^{1/2},\\ \mathscr{H}^{1/2}_{-1/2}(\beta_e F_e)=\frac{2}{3}(\beta_e F_e),\end{gathered} \tag{17}$$

and

$$\mathscr{D}\approx\mathscr{D}^0_e\mathscr{D}^0_h\frac{\frac{2}{3}\beta_e F_e+1}{\mathscr{D}^0_h(4/3\sqrt{\pi})(\beta_e F_e)^{1/2}+\mathscr{D}^0_e}. \tag{18}$$

Since $\mathscr{D}^0_e\gg\mathscr{D}^0_h$ and under our high injection conditions as specified previously Eq. (18) can be simplified to

$$\mathscr{D}\approx\mathscr{D}^0_h[\tfrac{2}{3}\beta_e F_e(t)+1]. \tag{18$'$}$$

Equations (18) and (18′) show that the ambipolar diffusion coefficient $\mathscr{D}$ decreases with an increase of distance from the crystal front surface because n decreases due to the absorption, and $F_e\sim n^{2/3}$.

Based on the model described above we can now explain the dependence of the PL decay rate on the emission energy. Let us examine the ratio

$$\eta(\omega,t)\equiv\frac{I(\omega,x=0,t)}{I(\omega,x=0,t=0)}$$

which characterizes the decrease with time of the luminescence at a frequency ω from a very thin layer near the surface. From Eq. (16), we obtain

$$\eta(\omega,t)=\frac{n_h(t)}{n_h(0)}\frac{\exp\left[\beta_e\left(\frac{m_h}{m_e+m_h}(\hbar\omega-E_g)-F_e(0)\right)\right]+1}{\exp\left[\beta_e\left(\frac{m_h}{m_e+m_h}(\hbar\omega-E_g)-F_e(t)\right)\right]+1}. \tag{19}$$

Thus, for the lower PL energies (''red frequencies''), satisfying the inequality

$$\frac{m_h}{m_e+m_h}(\hbar\omega-E_g)-F_e(t)<0 \tag{20}$$

and consequently

$$\frac{m_h}{m_e+m_h}(\hbar\omega-E_g)-F_e(0)<0,$$

since $F_e(0)>F_e(t)$,

$$\eta(\omega,t)\approx\frac{n_h(t)}{n_h(0)}. \tag{21}$$

Hence, the decrease of the intensity at the red frequency PL is determined primarily by the decrease of the holes density n_h due to diffusion.

Downloaded¬30¬Mar¬2005¬to¬132.66.16.12.¬Redistribution¬subject¬to¬AIP¬license¬or¬copyright,¬see¬http://jap.aip.org/jap/copyright.jsp

For the higher-energy ''blue'' frequencies, satisfying the relation

$$\frac{m_h}{m_e+m_h}(\hbar\omega-E_g)=F_e(0)$$

and consequently

$$\frac{m_h}{m_e+m_h}(\hbar\omega-E_g)-F_e(0)>0,$$

$$\eta(\omega,t)\approx 2\frac{n_h(t)}{n_h(0)}\exp\left[-\beta\left(\frac{m_h}{m_e+m_h}(\hbar\omega-E_g)-F_e(t)\right)\right]. \tag{22}$$

Equation (22) shows an essentially faster decay of the blue frequencies with respect to red ones as can be seen from comparing Eqs. (21) and (22). This effect is enhanced at lower temperatures, since the degeneracy parameter $\beta_e F_e$ [Eq. (15)] is proportional to T^{-1}; this has been verified experimentally and will be reported elsewhere. Thus, we obtain a qualitative explanation for our experimental data shown in Fig. 2 and clarify why the standard ambipolar diffusion self-absorption model (see Fig. 3) did not agree with our results.

When the injection level increases (n increases) and/or the temperature decreases, the degeneracy of the hole system also becomes important and one must use the general expression given by Eq. (7) for $I(\hbar\omega,x,t)$. For a strongly degenerate hole system and for red PL frequencies satisfying the conditions

$$\frac{m_h}{m_e+m_h}(\hbar\omega-E_g)-F_h(t)>0, \tag{23}$$

$$\frac{m_h}{m_e+m_h}(\hbar\omega-E_g)-F_e(t)>0, \tag{24}$$

we obtain from Eq. (7) that $\eta(\omega,t)\approx$const. That is to say, that the increase in the degeneracy parameter results in slowing down of the red luminescence decay rate. This effect can be easily understood, since for a strongly degenerate gas the lowest states are occupied and the diffusion does not influence their occupancy. This effect will be reported in more detail elsewhere.

C. The nonparabolic correction

1. The nonparabolic correction for the quasi-Fermi levels

Using a simulation program, based on Eqs. (7)–(12), we were able to fit only our lower-energy data. However, when measuring luminescence at energies of ~0.3 eV above the bottom of the conduction band the nonparabolic correction to the Γ valley band structure must also be considered.

The nonparabolic correction has two contributions: The first is a change in the position of the quasi-Fermi level, and the second is a change of the effective diffusion coefficient. Following others[16–18] we used the first-order nonparabolic correction to the conduction band: $E(1+\alpha E)=\hbar^2k^2/2m$, where α is the nonparabolicity parameter given by: $\alpha=(1/E_g)[1-(m^*/m_0)]^2$ and is equal to 0.576 for GaAs. The density of states then becomes

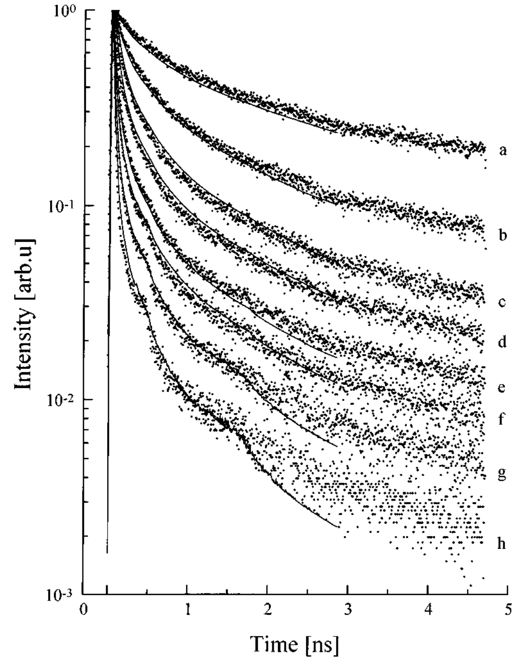

FIG. 5. Experimental time-resolved photoluminescence (dotted lines) and computer simulation (solid lines) of the thick 5 μm GaAs epilayer. The calculations are based on Fermi–Dirac carrier statistics and conduction-band nonparabolicity; the parameters used are given in Table I.

$$\nu(E)=\frac{\sqrt{2}}{\pi^2\hbar^3}m_e^{3/2}\sqrt{E}\sqrt{1+\alpha E}(1+2\alpha E)$$

$$\approx\frac{\sqrt{2}}{\pi^2\hbar^3}m_e^{3/2}\sqrt{E}\left(1+\frac{5\alpha E}{2}\right), \tag{25}$$

and hence the number of electrons in the conduction band is given by

$$n_e=\frac{(m_ek_BT_e)^{3/2}}{\sqrt{2}\pi^3\hbar^3}\left(\mathscr{F}_{1/2}(\beta_eF_e)+\frac{15\alpha k_BT_e}{4}\mathscr{F}_{3/2}(\beta_eF_e)\right). \tag{26}$$

This equation is used to calculate the quasi-Fermi level as a function of the electrons' density and temperature.

2. The nonparabolic correction for the diffusion coefficient

To calculate the new effective diffusion coefficient we use the Einstein relation in the nonparabolic regime,[17,18]

$$\frac{\mathscr{D}_e}{\mu_e}\approx\frac{k_BT_e}{q}\frac{\mathscr{F}_{1/2}(\beta_eF_e)+\frac{15}{4}\alpha k_BT_e\mathscr{F}_{3/2}(\beta_eF_e)}{\mathscr{F}_{-1/2}(\beta_eF_e)+\frac{15}{4}\alpha k_BT_e\mathscr{F}_{1/2}(\beta_eF_e)}, \tag{27}$$

where q is the electron charge. The carrier mobility is given by[11,12,19]

$$\mu_{e,h}=\frac{q\mathscr{D}^0_{e,h}}{k_BT_{e,h}}\mathscr{H}^0_{1/2}(\beta_{e,h}F_{e,h}). \tag{28}$$

This expression is obtained from the solution of the Boltzmann equation using the relaxation time approximation and

Downloaded¬30¬Mar¬2005¬to¬132.66.16.12.¬Redistribution¬subject¬to¬AIP¬license¬or¬copyright,¬see¬http://jap.aip.org/jap/copyright.jsp

assuming that the momentum relaxation time $\tau(E) \approx \tau_0 E^{-s}$ and $s = 1/2$. Following this procedure[20] we obtain the following expression for the electron mobility:

$$\mu_e = \frac{q \mathcal{D}_e^0}{k_B T_e} \frac{\mathcal{F}_0(\beta_e F_e) + \frac{7}{2} \alpha k_B T_e \mathcal{F}_1(\beta_e F_e)}{\mathcal{F}_{1/2}(\beta_e F_e) + \frac{15}{4} \alpha k_B T_e \mathcal{F}_{3/2}(\beta_e F_e)}. \tag{29}$$

Combining the expressions for the electron and hole mobilities with the Einstein relation gives the diffusion coefficients of electrons and holes, respectively,

$$\mathcal{D}_e = \frac{k_B T_e}{q} \mu_e^0 \frac{\mathcal{F}_0(\beta_e F_e) + \frac{7}{2} \alpha k_B T_e \mathcal{F}_1(\beta_e F_e)}{\mathcal{F}_{-1/2}(\beta_e F_e) + \frac{15}{4} \alpha k_B T_e \mathcal{F}_{1/2}(\beta_e F_e)},$$

$$\mathcal{D}_h = \frac{k_B T_h}{q} \mu_h^0 \mathcal{H}_0^{-1/2}(\beta_h F_h). \tag{30}$$

The new ambipolar diffusion coefficient then becomes

$$\mathcal{D} = \mathcal{D}_e^0 \mathcal{D}_h^0 \frac{\dfrac{T_h \mathcal{H}_{-1/2}^{1/2}(\beta_h F_h)}{1 + \frac{15}{4} \alpha k_B T_e \mathcal{H}_{1/2}^{3/2}(\beta_e F_e)} + \dfrac{T_e}{\mathcal{H}_{1/2}^{-1/2}(\beta_e F_e) + \frac{15}{4} \alpha k_B T_e}}{\dfrac{\mathcal{D}_e^0 T_h \mathcal{H}_0^{1/2}(\beta_h F_h)}{1 + \frac{15}{4} \alpha k_B T_e \mathcal{H}_{1/2}^{3/2}(\beta_e F_e)} + \dfrac{\mathcal{D}_h^0 T_e}{\mathcal{H}_{1/2}^0(\beta_e F_e) + \frac{7}{2} \alpha k_B T_e \mathcal{H}_{1/2}^1(\beta_e F_e)}}. \tag{31}$$

This new expression reduces to Eq. (12) when $\alpha = 0$ (the parabolic band approximation).

By using the approximation of $\beta_e F_e(x,t)$ from Eq. (15) and the simplified expression for the diffusion coefficient, Eq. (18′), one can see that $\mathcal{D} \approx 3.5 \mathcal{D}_h^0$ at the degenerate regime. However, at the nondegenerate regime $\mathcal{D} \approx 2 \mathcal{D}_h^0$, meaning that the effective diffusion coefficient varies in our case from ~14 to ~8 cm^2/s as function of the electron quasi Fermi level-F_e.

V. COMPARISON WITH THE EXPERIMENTAL RESULTS

Calculations of the TRPL spectra in the degenerate regime were performed using a simulation program based on an algorithm developed by Kosloff and Tal-Ezer.[21] This approach was originally used to solve Shrödinger equation and was later modified by Agmon *et al.* to solve the diffusion equation;[22,23] we implied the same approach for the semiconductor transport equations with Fermi–Dirac carrier distributions and nonparabolic conduction band.

In short, the numerical algorithm can be applied for any PDE having the form $\partial f / \partial t = \hat{L} f$, where L is a space-dependent operator; the solution is then given by

$$f(r, t + \Delta t) = \exp(-\Delta t \hat{L}) f(r, t). \tag{32}$$

In our case the operator L is the ambipolar diffusion equation, i.e.,

TABLE I. The parameters used in the calculations of the TRPL curves (solid lines) of Fig. 6.

Band-gap energy	$E_{gap} = 1.425$ eV
Electron effective mass	$m_e^* = 0.068 m_e$
Hole effective mass	$m_h^* = 0.512 m_e$
Total number of carriers generated by the excitation	$n(t=0) = 3 \times 10^{18}$ cm^{-3}
Hole diffusion coefficient	$D_h^0 = 4$ cm^2/s
Electron diffusion coefficient	$D_e^0 = 100$ cm^2/s
Absorption length at laser wavelength (595 nm)	2000 Å
Lattice temperature	$T_L = 300$ K
Initial electron temperature	$T_e(t=0) = 400$ K
Time constant for electron cooling	$\tau_c = 2$ ps
Nonradiative lifetime	350 ns
Radiative rate constant (at band-gap energy)	$B = 2 \times 10^{-10}$ cm^3/s
Interface recombination velocity	$S = 100$ cm/s
PL wavelength (nm):	Absorption length (cm)
710	4.3×10^{-5}
730	5.1×10^{-5}
750	6.0×10^{-5}
770	6.6×10^{-5}
790	7.1×10^{-5}
810	7.6×10^{-5}
830	8.3×10^{-5}
850	10.7×10^{-5}
870	12.4×10^{-5}

Downloaded¬30¬Mar¬2005¬to¬132.66.16.12.¬Redistribution¬subject¬to¬AIP¬license¬or¬copyright,¬see¬http://jap.aip.org/jap/copyright.jsp

$$\hat{L}=\frac{\partial}{\partial x}\left(D\,\frac{\partial}{\partial x}\right)+\mathcal{G}-\mathcal{R}, \tag{33}$$

where D is the ambipolar diffusion coefficient given by Eq. (31).

Our simulation starts by assuming an initial carrier distribution at $t=0$ that obeys the Beer–Lambert absorption law, the quasi-Fermi levels $F_e[x,t,T_e(t)]$, $F_h(x,t,T_h)$ are then found by numericaly solving Eq. (26) at each time step, and are then used to calculate D. D is then used to calculate the new distribution of the carriers at $t=t+\Delta t$ where Δt is the time step; this procedure is then repeated to the desired time period. Once the quasi-Fermi levels, $F_e[x,t,T_e(t)]$ and $F_h(x,t,T_h)$, are known, calculating the energy spectra at different times is a straightforward task. The electron cooling was introduced qualitively as an exponentially decaying process [see Eq. (5)] with a time constant of about 2–5 ps.

Figure 5 shows calculated TRPL curves of the thick sample on top of the experimental data of Fig. 2. The breaks seen in the data curves (g) and (h) are again due to IRF effects; similar breaks are also observed in the corresponding calculated curves due to convolution with the experimental IRF. The computer simulation is based on Eqs. (7), (9), (11), (26), (31), and (33). The initial total carrier density at $x=0$ and $t=0$ was estimated to be $n_e(0,0)=n_h(0,0)=3\times 10^{18}$ cm^{-3}, based on the laser power and the spot size on the irradiated sample; the other parameters used in the calculations are given in Table I. The observed agreement with the experimental results is very good; this means that the electron degeneracy and conduction-band nonparabolicity are the main factors responsible for the change in the PL decay rate at super band-gap energies.

Figures 6(a) and 6(b) show calculated PL versus energy spectra for the thin and thick samples, respectively, at various times following the excitation. These figures show a very pronounced change in the slope of the PL versus energy curves in both cases. At photon energies such that E_e and E_h are well above their respective quasi-Fermi energies the luminescence intensity I_{PL} is given by[5]

$$I_{\mathrm{PL}}\propto \exp[-(\hbar\omega-E_g)/k_BT]. \tag{34}$$

Thus the slope of the I_{PL} vs $\hbar\omega$ on a semilogarithmic plot is a measure of the electron temperature. In the case of the thin crystal the slope is almost constant at $t>20$ ps; however, in the case of the thick sample [Fig. 6(b)], the slope still changes at $t>50$ ps. These slope changes are not due to electron cooling but rather due to an enhanced diffusion of the high energy carriers as a result of both carrier degeneracy and band nonparabolicity.

This emphasizes the importance of diffusion in obtaining correct carrier energy loss rates using TRPL methods. It means that diffusion and/or transport must be considered whenever the sample is not too thin (>0.5 μm) or the transport is slow. The later is very important in multiquantum-well and superlattice structures since the carrier vertical transport is slower than in the bulk; in these quantum confined structures the transport must be considered also for very thin samples ($\leqslant 0.5$ μm).

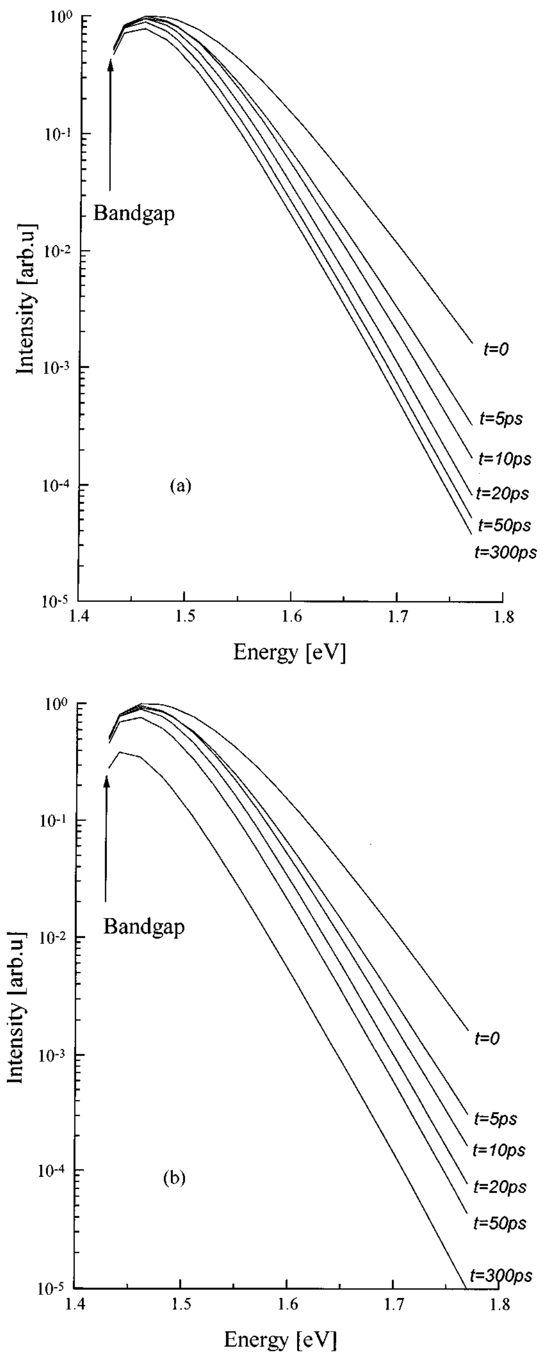

FIG. 6. (a) Energy-resolved spectra of the thin crystal calculated at several times following the excitation: $t=0$, 5, 10, 20, 50, and 300 ps. The observed change in the slope at the high energies at $t>10$ ps is due to transport effects. (b) Energy-resolved spectra of the thick crystal calculated at several times following the excitation: $t=0$, 5, 10, 20, 50, and 300 ps. The observed change in the slope at the high energies at $t>10$ ps is due to transport effects.

VI. SUMMARY AND CONCLUSIONS

In this work we have shown that transport effects play a central role in the super band-gap luminescence spectra of degenerate semiconductors. We developed a rigorous numerical model which calculates the super band-gap time-resolved luminescence spectra under degenerate carrier conditions and nonparabolic band structure; the model showed

Downloaded¬30¬Mar¬2005¬to¬132.66.16.12.¬Redistribution¬subject¬to¬AIP¬license¬or¬copyright,¬see¬http://jap.aip.org/jap/copyright.jsp

excellent agreement with our experimental results. The degeneracy causes a much faster decay of the high-energy emmision with respect to the lower energy (closer to the band gap) emission. These transport phenomena affect the energy-resolved spectra in a similar way to carrier cooling effects; therefore, they must be taken into account in the interpretation of experiments studying degenerate electron–hole plasma cooling in semiconductor using TRPL methods.

[1] A. J. Shah, Solid-State Electron. **32**, 1051 (1989); Superlattices Microstruct. **6**, 293 (1989); *Hot Carriers in Semiconductor Nanostructures* (Academic, New York, 1992); B. C. L. Tang, F. W. Wises, and D. Edelstein, Optoelectronics **1**, 153 (1986).
[2] A. Y. Rosenwaks, L. Burstein, Y. Shapira, and D. Huppert, J. Phys. Chem. **94**, 6842 (1990); Appl. Phys. Lett. **57**, 458 (1990); B. P. Besler-Podorowsky, D. Huppert, Y. Rosenwaks, and Y. Shapira, J. Phys. Chem. **95**, 4370 (1991).
[3] A. Y. Rosenwaks, Y. Shapira, and D. Huppert, Phys. Rev. B **44**, 13 097 (1991); B. Y. Rosenwaks, Y. Shapira, and D. Huppert, *ibid.* **45**, 9108 (1992); C. M. Evenor, S. Gottesfield, Z. Harzion, D. Huppert, and S. W. Feldberg, J. Phys. Chem. **88**, 6213 (1984).
[4] Y. Rosenwaks, B. R. Thacker, R. K. Ahrenkiel, and A. J. Nozik, J. Phys. Chem. **96**, 10 096 (1995).
[5] S. A. Lyon, J. Lumin. **35**, 121 (1986).
[6] Z. Y. Xu and C. L. Tang, Appl. Phys. Lett. **44**, 692 (1984); D. C. Edelstein, C. L. Tang, A. J. Nozik, *ibid.* **51**, 48 (1987).
[7] D. W. Bailey and C. J. Stanton, Appl. Phys. Lett. **40**, 880 (1992).
[8] C. A. Parsons, B. R. Thacker, D. M. Szmyd, M. W. Peterson, W. E. McMahon, and A. J. Nozik, J. Chem. Phys. **93**, 7706 (1990).
[9] Y. Rosenwaks, Y. Shapira, and D. Huppert, Appl. Phys. Lett. **57**, 2552 (1990).
[10] A. Mooradian and H. M. Fain, Phys. Rev. **148**, 873 (1966).
[11] A. Othonos, H. M. van Driel, J. F. Young, and P. J. Kelly, Phys. Rev. B **43**, 6682 (1991).
[12] J. F. Young and H. M. van Driel, Phys. Rev. B **26**, 2147 (1982).
[13] S. E. Esipov and V. B. Levinson, Adv. Phys. **36**, 331 (1987).
[14] P. Lugli, C. Jacoboni, P. Kocavar, and P. Reggiani, Proc. SPIE **793**, 102 (1987).
[15] A. I. Anselm, *Introduction to the Theory of Semiconductors* (Moscow, 1978) (in Russian).
[16] J. Shah, *Hot Carriers in Semiconductors* (Academic, New York, 1992).
[17] A. N. Chakravarti and B. R. Nag, Int. J. Electron. **37**, 281 (1974).
[18] B. R. Nag, *Theory of Electrical Transport in Semiconductors* (Pergamon, Oxford, 1972).
[19] H. M. van Driel, Phys. Rev. B **35**, 8166 (1987).
[20] M. Sure, *Physics of Semiconductors Devices* (Prentice–Hall, Englewood Cliffs, NJ, 1990); C. M. Wolfe, N. Holonyac, Jr., and G. E. Stillman, *Physical Properties of Semiconductors* (Prentice–Hall, Englewood Cliffs, NJ, 1989).
[21] R. Kosloff and H. Tal-Ezer, Chem. Phys. Lett. **127**, 223 (1986).
[22] N. Agmon and R. Kosloff, J. Phys. Chem. **91**, 1988 (1987).
[23] E. Pines, D. Huppert, and N. Agmon, J. Chem. Phys. **88**, 5620 (1988).

Downloaded¬30¬Mar¬2005¬to¬132.66.16.12.¬Redistribution¬subject¬to¬AIP¬license¬or¬copyright,¬see¬http://jap.aip.org/jap/copyright.jsp